INTERNATIONAL JOURNAL FOR NUMERICAL METHODS IN FLUIDS
Int. J. Numer. Meth. Fluids 2003; **42**:741–763 (DOI: 10.1002/fld.552)

Dispersion and stability analyses of the linearized two-dimensional shallow water equations in boundary-fitted co-ordinates

S. Sankaranarayanan*,† and Malcolm L. Spaulding

Department of Ocean Engineering, University of Rhode Island, Narragansett, RI-02882, U.S.A.

SUMMARY

In the present investigation, a Fourier analysis is used to study the phase and group speeds of a linearized, two-dimensional shallow water equations, in a non-orthogonal boundary-fitted co-ordinate system. The phase and group speeds for the spatially discretized equations, using the second-order scheme in an Arakawa C grid, are calculated for grids with varying degrees of non-orthogonality and compared with those obtained from the continuous case. The spatially discrete system is seen to be slightly dispersive, with the degree of dispersivity increasing with an decrease in the grid non-orthogonality angle or decrease in grid resolution and this is in agreement with the conclusions reached by Sankaranarayanan and Spaulding (*J. Comput. Phys.*, 2003; **184**:299–320). The stability condition for the non-orthogonal case is satisfied even when the grid non-orthogonality angle, is as low as 30° for the Crank Nicolson and three-time level schemes. A two-dimensional wave deformation analysis, based on complex propagation factor developed by Leendertse (Report RM-5294-PR, The Rand Corp., Santa Monica, CA, 1967), is used to estimate the amplitude and phase errors of the two-time level Crank–Nicolson scheme. There is no dissipation in the amplitude of the solution. However, the phase error is found to increase, as the grid angle decreases for a constant Courant number, and increases as Courant number increases. Copyright © 2003 John Wiley & Sons, Ltd.

KEY WORDS: stability; dispersion; boundary-fitted grids; compact difference; non-orthogonality

1. INTRODUCTION

Sankaranarayanan and Spaulding [1] analysed the accuracy of the finite difference approximations of the linearized shallow water equations in a non-orthogonal boundary-fitted co-ordinate system (BFC) using a truncation error analysis. Expressing the co-ordinate metrics in BFC, in terms of the grid quality parameters, such as aspect ratio and grid non-orthogonality, they

*Correspondence to: S. Sankaranarayanan, Applied Science Associates Inc., 70 Dean Knauss Drive, Narragansett, RI-02882, U.S.A.
†E-mail: subbayya@appsci.com

Contract/grant sponsor: University of Rhode Island

Received 15 February 2002
Accepted 7 October 2002

showed that the coefficient of the truncation error terms is dependent on the grid angle and the aspect ratio. However it is difficult to give an estimate of the truncation error, since the higher order derivatives in the truncation error terms, in a non-orthogonal BFC system become very cumbersome for numerical evaluation. They also found that the error in model predicted currents were found to increase with the decrease in grid angle or grid resolution.

The dispersion and stability analyses for the various schemes used in solving shallow water equations have been carried out in the past using a Fourier analysis of the differencing techniques, solving the governing equations in a Cartesian co-ordinate system [2]. Foreman [3] determined the accuracy of some finite difference and finite element techniques, by comparing the numerical and analytical plane wave solutions using Fourier analysis. Song and Tang [4] analysed the dispersion and group velocity for linearized, three-dimensional shallow water equations, discretized using a hybrid scheme based on Arakawa's B and C spatial grid types. Leendertse [5] used a complex propagation factor to compare the amplitude and phase components of the Fourier series representing the computed wave calculated from the fully discretized equations with that of the real wave.

The accuracy of a given finite difference scheme is evaluated by using a Fourier analysis of the semi-discrete and continuous systems. The stability and dispersion analyses usually require linearized equations with constant depth on a regular grid. Since the present study involves an analysis of the linearized shallow water equations in a non-orthogonal BFC system, the numerical and analytical plane wave solution of the system is performed in the transformed plane. The co-ordinate metrics such $g^{(11)}, g^{(12)}, g^{(22)}$ and the Jacobian J that appear in these solutions are approximated using centered finite difference approximations. The amplitude and phase errors of the fully discretized equations are also computed using the complex propagation factor [5], for the schemes used in this study.

2. GOVERNING EQUATIONS

Using a spherical co-ordinate system, where ϕ is the longitude, θ is the latitude, R is the mean radius of the earth, the two-dimensional vertically averaged continuity equation is given by [6]

$$\frac{\partial \zeta}{\partial t} + \frac{1}{R\cos\theta}\frac{\partial UD}{\partial \phi} + \frac{1}{R}\frac{\partial VD}{\partial \theta} - \frac{VD}{R}\tan\theta = 0 \tag{1}$$

where U and V are the vertically averaged velocities in the ϕ and θ directions, ζ is the water surface elevation, D is total depth $(\zeta + h)$, and h is the water depth. Neglecting the advective, viscous, and Coriolis terms, the momentum equation in the ϕ-direction is given by

$$\frac{\partial UD}{\partial t} = -\frac{gD}{R\cos\theta}\left(\frac{\partial \zeta}{\partial \phi}\right) \tag{2}$$

Similarly, the momentum equation in the θ-direction is given by

$$\frac{\partial VD}{\partial t} = -\frac{gD}{R}\left(\frac{\partial \zeta}{\partial \theta}\right) \tag{3}$$

Coriolis effects have been neglected and hence our analysis will be applicable to problems where Rossby ($V/(\Omega L)$) number is less than 1, where V is the velocity of flows, Ω is the angular velocity of the earth and L is the length scale of motion [7].

2.1. Governing equations in the BFC system

The linearized transformed equations of motion, in terms of the contravariant velocities (U^c and V^c) in the curvilinear co-ordinate system (ξ, η) are given by
Continuity equation

$$\frac{\partial \zeta}{\partial t} + \frac{(\sqrt{G}U^c D)_\xi + (\sqrt{G}V^c D)_\eta}{R\sqrt{G}} = 0 \tag{4}$$

Momentum equation in ξ-direction

$$\frac{\partial (DU^c)}{\partial t} + \frac{gD(g^{(11)}\zeta_\xi + g^{(12)}\zeta_\eta)}{R} = 0 \tag{5}$$

Momentum equation in η-direction

$$\frac{\partial (DV^c)}{\partial t} + \frac{gD(g^{(21)}\zeta_\xi + g^{(22)}\zeta_\eta)}{R} = 0 \tag{6}$$

$g^{(ij)}$ is the inverse metric tensor given by

$$g^{(ij)} = \frac{1}{G}\begin{pmatrix} \phi_\eta\phi_\eta \cos^2\theta + \theta_\eta\theta_\eta & -(\phi_\xi\phi_\eta \cos^2\theta + \theta_\xi\theta_\eta) \\ -(\phi_\xi\phi_\eta \cos^2\theta + \theta_\xi\theta_\eta) & \phi_\xi\phi_\xi \cos^2\theta + \theta_\xi\theta_\xi \end{pmatrix} \tag{7}$$

where G is the determinant of the metric tensor g_{ij}

$$G = J^2 \cos^2\theta \tag{8}$$

and J is the Jacobian of the transformation given by

$$J = \phi_\xi\theta_\eta - \phi_\eta\theta_\xi \tag{9}$$

$g_{(ij)}$ is the metric tensor and is given by

$$g_{(ij)} = \begin{pmatrix} \phi_\xi\phi_\xi \cos^2\theta + \theta_\xi\theta_\xi & \phi_\xi\phi_\eta \cos^2\theta + \theta_\xi\theta_\eta \\ \phi_\xi\phi_\eta \cos^2\theta + \theta_\xi\theta_\eta & \phi_\eta\phi_\eta \cos^2\theta + \theta_\eta\theta_\eta \end{pmatrix} \tag{10}$$

and the subscripted variables ($\phi_\xi, \phi_\eta, \theta_\xi$ and θ_η) refer to the derivatives with respect to the subscripts indicated.

3. DISPERSION ANALYSIS

Taking the case of a constant total depth, 'D' and assuming the grid to be uniform, the following change of variables is performed, so that the governing equations are amenable to Fourier analysis: $\sqrt{G}U^c = \hat{U}$, $\sqrt{G}V^c = \hat{V}$, $\hat{Z} = \zeta\sqrt{g/D}$, $c = \sqrt{gD}$. The governing equations then become,

Continuity equation

$$\frac{\partial \hat{Z}}{\partial t} + \frac{c\hat{U}_\xi + c\hat{V}_\eta}{R\sqrt{G}} = 0 \tag{11}$$

Momentum equation in ξ-direction

$$\frac{\partial \hat{U}}{\partial t} + \frac{c\sqrt{G}(g^{(11)}\hat{Z}_\xi + g^{(12)}\hat{Z}_\eta)}{R} = 0 \tag{12}$$

Momentum equation in η-direction

$$\frac{\partial \hat{V}}{\partial t} + \frac{c\sqrt{G}(g^{(12)}\hat{Z}_\xi + g^{(22)}\hat{Z}_\eta)}{R} = 0 \tag{13}$$

where the subscripted variables ($\hat{U}_\xi, \hat{V}_\eta, \hat{Z}_\xi$ and $\hat{Z}_\eta$) refer to the partial derivatives with respect to the subscripts indicated.

3.1. Dispersion analysis of the continuous BFC system

A continuous Fourier mode is introduced in each field variable such that,

$$\begin{aligned} \hat{U} &= U_0 \mathrm{e}^{i[k_\xi \xi + k_\eta \eta - \omega t]} \\ \hat{V} &= V_0 \mathrm{e}^{i[k_\xi \xi + k_\eta \eta - \omega t]} \\ \hat{Z} &= Z_0 \mathrm{e}^{i[k_\xi \xi + k_\eta \eta - \omega t]} \end{aligned} \tag{14}$$

Equations (11) through (13) reduce to,

$$\begin{pmatrix} -\frac{\mathrm{i}\omega}{\sqrt{\mathrm{G}}} & 0 & \frac{\mathrm{i}c(g^{(11)}k_\xi + g^{(12)}k_\eta)}{R} \\ 0 & -\frac{\mathrm{i}\omega}{\sqrt{\mathrm{G}}} & \frac{\mathrm{i}c(g^{(21)}k_\xi + g^{(22)}k_\eta)}{R} \\ \frac{\mathrm{i}ck_\xi}{\sqrt{\mathrm{G}}R} & \frac{\mathrm{i}ck_\eta}{\sqrt{\mathrm{G}}R} & -\mathrm{i}\omega \end{pmatrix} \begin{pmatrix} U_0 \\ V_0 \\ Z_0 \end{pmatrix} = 0 \tag{15}$$

where k_ξ and k_η are the wave numbers in the ξ and η directions, respectively.

A non-trivial solution of Equation (15) requires that

$$\mathrm{i}R^2\omega^3 + \mathrm{i}c^2(-2k_\xi g^{(12)}k_\eta - k_\eta^2 g^{(22)} - k_\xi^2 g^{(11)})\omega = 0 \tag{16}$$

Solution of Equation (16) gives three frequencies.

$$\omega = \left\{0, \frac{c\sqrt{s_3}}{R}, -\frac{c\sqrt{s_3}}{R}\right\} \tag{17}$$

where $s_3 = 2\,g^{(12)}k_\xi k_\eta + g^{(22)}k_\eta^2 + g^{(11)}k_\xi^2$.

The first of the waves given by Equation (17) represents a steady-state flow field, while the other two represent, progressive and retrogressive waves, respectively. The corresponding frequencies in the continuous system in Cartesian co-ordinates, can be obtained by substituting the following equations in Equation (17):

$$k_\xi^2 = (k_x\,\mathrm{d}x)^2, \quad k_\eta^2 = (k_y\,\mathrm{d}x)^2, \quad R = 1, \quad g^{(11)} = 1, \quad g^{(12)} = 0, \quad g^{(22)} = 1 \tag{18}$$

The group velocity CG_ξ, corresponding to the values of ω in Equation (17) is given by

$$CG_\xi = \frac{d\omega}{dk_\xi} = \left\{0, \frac{c(k_\eta g^{(12)} + k_\xi g^{(11)})}{R\sqrt{s_3}}, -\frac{c(k_\eta g^{(12)} + k_\xi g^{(11)})}{R\sqrt{s_3}}\right\} \tag{19}$$

The corresponding expression for group speed in the continuous system for Cartesian co-ordinates can be obtained by substituting Equation (18) into Equation (19).

3.2. Dispersion analysis of the spatially discrete BFC system

In the present study, the second-order spatial discretization on an Arakawa C grid [2], used in Muin and Spaulding [6] has been selected, for analysing the dispersion of the difference scheme in a BFC system.

The spatially discretized equations, on an Arakawa-C grid are given by
Continuity equation

$$\left(\frac{d\hat{Z}}{dt}\right)_{j,m} + c\,\frac{(\hat{U}^{n+1}_{j+1/2,m} - \hat{U}^{n+1}_{j-1/2,m})}{R\sqrt{G}\,d\xi} + c\,\frac{(\hat{V}^{n+1}_{j,m+1/2} - \hat{V}^{n+1}_{j,m-1/2})}{R\sqrt{G}\,d\eta} = 0 \tag{20}$$

ξ-momentum equation

$$\left(\frac{d\hat{U}}{dt}\right)_{j,m} + \frac{c\sqrt{G}g^{(11)}(\hat{Z}_{j+1,m} - \hat{Z}_{j,m})^{n+1}}{R\,d\xi} + \frac{c\sqrt{G}g^{(12)}(\hat{Z}_{j+1,m+1} + \hat{Z}_{j,m+1} - \hat{Z}_{j+1,m-1} - \hat{Z}_{j,m-1})^{n+1}}{4R\,d\eta} = 0 \tag{21}$$

η-momentum equation

$$\left(\frac{d\hat{V}}{dt}\right)_{j,m} + \frac{c\sqrt{G}g^{(22)}(\hat{Z}_{j,m+1} - \hat{Z}_{j,m})^{n+1}}{R\,d\eta} + \frac{c\sqrt{G}g^{(12)}(\hat{Z}_{j+1,m+1} + \hat{Z}_{j+1,m} - \hat{Z}_{j-1,m+1} - \hat{Z}_{j-1,m})^{n+1}}{4R\,d\xi} = 0 \tag{22}$$

It should be noted that the third term in Equations (21) and (22), which use a non-compact stencil is due to the non-orthogonality of the grid. Sankaranarayanan and Spaulding [1] have shown through a truncation error analysis that the error in this term increases as the grid angle decreases from 90°.

A spatially discrete Fourier mode is introduced for each field variable such that:

$$\begin{aligned}\hat{U}_{j,m} &= U_0 e^{i[jk_\xi\,d\xi + mk_\eta\,d\eta - \omega t]}\\ \hat{V}_{j,m} &= V_0 e^{i[jk_\xi\,d\xi + mk_\eta\,d\eta - \omega t]}\\ \hat{Z}_{j,m} &= Z_0 e^{i[jk_\xi\,d\xi + mk_\eta\,d\eta - \omega t]}\end{aligned} \tag{23}$$

Assuming $\mathrm{d}\eta = \mathrm{d}\xi$, Equations (20) through (22) reduce to,

$$\begin{pmatrix} -\frac{\mathrm{i}\,\omega}{\sqrt{\mathrm{G}}} & 0 & \mathrm{i}\,c\,p_1 \\ 0 & -\frac{\mathrm{i}\,\omega}{\sqrt{\mathrm{G}}} & \mathrm{i}c\,p_2 \\ \frac{2\,\mathrm{i}\,c\,\sin(k_\xi/2)}{\sqrt{\mathrm{G}}\,R\,\mathrm{d}\xi} & \frac{2\,\mathrm{i}\,c\,\sin(k_\eta/2)}{\sqrt{\mathrm{G}}\,R\,\mathrm{d}\xi} & -\mathrm{i}\,\omega \end{pmatrix} \begin{pmatrix} U_0 \\ V_0 \\ Z_0 \end{pmatrix} = 0 \tag{24}$$

where

$$\begin{aligned} p_1 &= \frac{2\,g^{(11)}\,\sin(k_\xi/2) + g^{(12)}\,\sin k_\eta\,\cos(k_\xi/2)}{R\,\mathrm{d}\xi} \\ p_2 &= \frac{g^{(21)}\,\cos(k_\eta/2)\,\sin k_\xi + 2\,g^{(22)}\,\sin(k_\eta/2)}{R\,\mathrm{d}\xi} \end{aligned} \tag{25}$$

Assuming $\mathrm{d}\xi = \mathrm{d}\eta$, a non-trivial solution of Equation (24) requires that

$$\begin{aligned} &\mathrm{i}\,R^2\,(\mathrm{d}\xi)^2\omega^3 - \left(2\,\mathrm{i}g^{(12)}c^2\,\sin k_\eta\,\sin k_\xi - 4\mathrm{i}g^{(11)}c^2\,\sin^2\frac{k_\xi}{2}\right. \\ &\left. - 4\mathrm{i}g^{(22)}c^2\,\sin^2\frac{k_\eta}{2}\right)\omega = 0 \end{aligned} \tag{26}$$

It is noted that $\mathrm{d}\xi = \mathrm{d}\eta = 1$ in the transformed plane.

Solution of Equation (26) gives three frequencies:

$$\omega = \left\{0, \pm\frac{\sqrt{2}c\sqrt{2p + 2q + s}}{R\,\mathrm{d}\xi}\right\} \tag{27}$$

where

$$p = g^{(11)}\,\sin^2\frac{k_\xi}{2}, \quad q = g^{(22)}\,\sin^2\frac{k_\eta}{2}, \quad s = g^{(12)}\,\sin k_\xi\,\sin k_\eta \tag{28}$$

The group velocity CG_ξ, corresponding to the values of ω in Equation (27), is given by,

$$\mathrm{CG}_\xi = \frac{\mathrm{d}\omega}{\mathrm{d}k_\xi} = \left\{0, \pm\frac{cs_1}{R\sqrt{2(2p + 2q + s)}}\right\} \tag{29}$$

where $s_1 = g^{(11)}\,\sin(k_\xi) + g^{(12)}\,\sin(k_\eta)\,\cos(k_\xi)$ substituting $d\xi = \mathrm{d}x$ and using Equation (18) the expressions for frequency and group speeds, for the three-point, second-order spatial discretization in Cartesian co-ordinates can be obtained.

4. STABILITY ANALYSIS

A stability analysis of the Equations (20) through (22) is performed by using the classical von Neumann method, under the assumption that the governing equations are defined on an

infinite spatial domain, or with periodic boundary conditions on a finite domain. Applying a generalized second-order scheme in space and time to Equations (20) through (22) gives,
Continuity equation

$$\frac{(1+\beta)\hat{Z}_{j,m}^{n+1}-(2\beta+1)\hat{Z}_{j,m}^{n}+\beta\hat{Z}_{j,m}^{n-1}}{\mathrm{d}t}+(1-\theta)c\,\frac{(\hat{U}_{j+1/2,m}^{n+1}-\hat{U}_{j-1/2,m}^{n+1})}{R\sqrt{G}\,\mathrm{d}\xi}$$
$$+\theta c\,\frac{(\hat{U}_{j+1/2,m}^{n}-\hat{U}_{j-1/2,m}^{n})}{R\sqrt{G}\,\mathrm{d}\xi}+(1-\theta)c\,\frac{(\hat{V}_{j,m+1/2}^{n+1}-\hat{V}_{j,m-1/2}^{n+1})}{R\sqrt{G}\,\mathrm{d}\eta}$$
$$+\theta c\,\frac{(\hat{V}_{j,m+1/2}^{n}-\hat{V}_{j,m-1/2}^{n})}{R\sqrt{G}\,\mathrm{d}\eta}=0 \tag{30}$$

ξ-momentum equation

$$\frac{(1+\beta)\hat{U}_{j+1/2,m}^{n+1}-(2\beta+1)\hat{U}_{j+1/2,m}^{n}+\beta\hat{U}_{j+1/2,m}^{n-1}}{\mathrm{d}t}$$
$$+\frac{c(1-\theta)\sqrt{G}g^{(11)}(\hat{Z}_{j+1,m}-\hat{Z}_{j,m})^{n+1}}{R\,\mathrm{d}\xi}+\frac{c\,\theta\sqrt{G}g^{(11)}(\hat{Z}_{j+1,m}-\hat{Z}_{j,m})^{n}}{R\,\mathrm{d}\xi}$$
$$+\frac{c(1-\theta)\sqrt{G}g^{(12)}(\hat{Z}_{j+1,m+1}+\hat{Z}_{j,m+1}-\hat{Z}_{j+1,m-1}-\hat{Z}_{j,m-1})^{n+1}}{4R\,\mathrm{d}\eta}$$
$$+\frac{c\,\theta\sqrt{G}g^{(12)}(\hat{Z}_{j+1,m+1}+\hat{Z}_{j,m+1}-\hat{Z}_{j+1,m-1}-\hat{Z}_{j,m-1})^{n}}{4R\,\mathrm{d}\eta}=0 \tag{31}$$

η-momentum equation

$$\frac{(1+\beta)\hat{U}_{j,m+1/2}^{n+1}-(2\beta+1)\hat{U}_{j,m+1/2}^{n}+\beta\hat{U}_{j,m+1/2}^{n-1}}{\mathrm{d}t}$$
$$+\frac{c(1-\theta)\sqrt{G}g^{(22)}(\hat{Z}_{j,m+1}-\hat{Z}_{j,m})^{n+1}}{R\,\mathrm{d}\eta}+\frac{c\,\theta\sqrt{G}g^{(22)}(\hat{Z}_{j,m+1}-\hat{Z}_{j,m})^{n}}{R\,\mathrm{d}\eta}$$
$$+\frac{c(1-\theta)\sqrt{G}g^{(12)}(\hat{Z}_{j+1,m+1}+\hat{Z}_{j+1,m}-\hat{Z}_{j-1,m+1}-\hat{Z}_{j-1,m})^{n+1}}{4R\,\mathrm{d}\xi}$$
$$+\frac{c\,\theta\sqrt{G}g^{(12)}(\hat{Z}_{j+1,m+1}+\hat{Z}_{j+1,m}-\hat{Z}_{j-1,m+1}-\hat{Z}_{j-1,m})^{n}}{4R\,\mathrm{d}\xi}=0 \tag{32}$$

where β and θ are the weighting factors for the second-order scheme.

After introducing the spatially and temporally discrete Fourier modes for all the variables as follows:

$$\begin{aligned}\hat{U}^n_{j,m} &= U_0 \mathrm{e}^{\mathrm{i}[jk_\xi \,\mathrm{d}\xi + mk_\eta \,\mathrm{d}\eta - n\omega \,\mathrm{d}t]} \\ \hat{V}^n_{j,m} &= V_0 \mathrm{e}^{\mathrm{i}[jk_\xi \,\mathrm{d}\xi + mk_\eta \,\mathrm{d}\eta - n\omega \,\mathrm{d}t]} \\ \hat{Z}^n_{j,m} &= Z_0 \mathrm{e}^{\mathrm{i}[jk_\xi \,\mathrm{d}\xi + mk_\eta \,\mathrm{d}\eta - n\omega \,\mathrm{d}t]}\end{aligned} \tag{33}$$

The fully discretized equations reduce to

$$\begin{pmatrix} \frac{(1+\beta)\lambda^2-(2\beta+1)\lambda+\beta}{\mathrm{d}tJ} & 0 & c\mathrm{i}\,p_1[\lambda^2(1-\theta)+\lambda\theta] \\ 0 & \frac{(1+\beta)\lambda^2-(2\beta+1)\lambda+\beta}{\mathrm{d}tJ} & c\mathrm{i}\,p_2[\lambda^2(1-\theta)+\lambda\theta] \\ \frac{2\mathrm{i}c\,\sin(k_\xi/2)[\lambda^2(1-\theta)+\lambda\theta]}{\mathrm{d}\xi JR} & \frac{2\mathrm{i}c\,\sin(k_\eta/2)[\lambda^2(1-\theta)+\lambda\theta]}{\mathrm{d}\eta JR} & \frac{(1+\beta)\lambda^2-(2\beta+1)\lambda+\beta}{\mathrm{d}tJ} \end{pmatrix} \begin{pmatrix} U_0 \\ V_0 \\ Z_0 \end{pmatrix} = 0 \tag{34}$$

where $\lambda = \mathrm{e}^{(\pm \mathrm{i}\omega \,\mathrm{d}t)}$ and represents the change in amplitude and phase over a time interval $\mathrm{d}t$.

Assuming $\mathrm{d}\eta = \mathrm{d}\xi$, a non-trivial solution of Equation (34) requires that

$$\begin{aligned}&(\lambda^4(-8\theta\, p_{13} + 4\theta^2 p_{13} + R^2\beta^2 + 4p_{13} + R^2 + 2R^2\beta) \\ &+ \lambda^3(8\theta p_{13} - 8\theta^2 p_{13} - 4R^2\beta^2 - 2R^2 - 6R^2\beta) \\ &+ \lambda^2(6R^2\beta^2 + 4\theta^2 p_{13} + R^2 + 6R^2\beta) \\ &+ \lambda(-2R^2\beta - 4R^2\beta^2) + R^2\beta^2)(\lambda^2 + \lambda^2\beta - 2\lambda\beta - \lambda + \beta) = 0\end{aligned} \tag{35}$$

where, $p_{13} = (p+q+s/2)\,c_0^2$, $p = g^{(11)} \sin^2(k_\xi/2)$, $q = g^{(22)} \sin^2(k_\eta/2)$ and $s = g^{(12)} \sin k_\xi \sin k_\eta$.

The three-time level temporal scheme given in Reference [6] for two dimensions can be obtained by substituting $\beta = 1/2$ and $\theta = 0$ in Equation (35). Thus for the three-time level scheme, Equation (35) reduces to,

$$(\lambda - 1)(3\lambda - 1)(a_1\lambda^4 - 24R^2\lambda^3 + 22R^2\lambda^2 - 8R^2\lambda + 1) = 0 \tag{36}$$

where $a_1 = 16\, p_{13} + 9\, R^2$.

Solution of Equation (36) gives six eigenvalues

$$\{\lambda\} = \begin{Bmatrix} \frac{6R^2 \pm a_2\sqrt{a_4 - a_5} - 2Ra_3}{a_1} \\ \frac{6R^2 \pm a_2\sqrt{a_4 + a_5} + 2a_3}{a_1} \\ 1 \\ \frac{1}{3} \end{Bmatrix} \tag{37}$$

where $a_2 = \sqrt[4]{1/9R^2 - a_1}$, $a_3 = \sqrt{9R^2 - a_1}$, $a_4 = a_3\,(72R^4 - 7a_1R^2)$, $a_5 = 216R^5 - 33a_1R^3 + a_1^2R$.

The eigenvalues for the same discretization in Cartesian co-ordinates, obtained by using the substitutions given in Equation (18), are identical to that given in Reference [8]. It seems very difficult to derive a stability criterion, from the eigenvalues given in Equation (37), since the characteristic equation for this scheme is a polynomial of sixth order. The eigenvalues can, however, be numerically evaluated for a given $\mathrm{d}t$, as discussed later.

Table I. Table of grid parameters.

Angle (γ) (deg)	$g_{(11)}$	$g_{(22)}$	$g_{(12)}$	J	AR
90	7.7648E − 09	7.7685E − 09	0	7.7666e − 09	1.0
60	8.5816E − 09	9.9139E − 09	−4.2908E − 09	9.2237E − 09	1.075
50	9.0392E − 09	1.2853E − 08	−6.7794E − 09	1.0779E − 08	1.192
30	1.0655E − 08	3.1743E − 08	−1.5983E − 08	1.8391E − 08	1.726

A two-time level, Crank–Nicolson scheme can be obtained by substituting $\beta = 0$ and $\theta = 1/2$ in Equations (30) through (32). The characteristic equation (Equation (35)) for Crank–Nicolson scheme then becomes

$$(p_{13} + R^2)\lambda^3 + (p_{13} - 3R^2)\lambda^2 + (-p_{13} + 3R^2)\lambda - (p_{13} + R^2) = 0 \tag{38}$$

where $p_{13} = c^2 \mathrm{d}t^2(p + q + s/2)$.

Solution of Equation (38) gives three eigenvalues

$$\lambda = \left\{ 1, \frac{p_{13}^2 - p_{13} + 2\sqrt{-R^2 p_{13}}}{R^2 + p_{13}}, \frac{p_{13}^2 - p_{13} - 2\sqrt{-R^2 p_{13}}}{R^2 + p_{13}} \right\} \tag{39}$$

If $p_{13} > 0$, Equation (39) can be written in the form

$$\lambda = \left\{ 1, \frac{p_{13}^2 - p_{13} + \mathrm{i}2\sqrt{R^2 p_{13}}}{R^2 + p_{13}}, \frac{p_{13}^2 - p_{13} - \mathrm{i}2\sqrt{R^2 p_{13}}}{R^2 + p_{13}} \right\} \tag{40}$$

$$|\lambda| = \{1, 1, 1\} \tag{41}$$

The eigenvalues for the same discretization in Cartesian co-ordinates can be obtained by using the substitutions given in Equation (18), and is identical to that given in Reference [8], for the Cartesian co-ordinates. The first of the eigenvalues given by $\lambda = 1$ is neutrally stable, while the other eigenvalues are found to be neutrally stable only when $M \geqslant 0$, then $(p + q) \geqslant -s/2$.

The stability requirement in the transformed co-ordinates, for the Crank–Nicolson scheme is given by

$$g^{(11)} \sin^2 \frac{k_\xi}{2} + g^{(22)} \sin^2 \frac{k_\eta}{2} \geqslant -\frac{g^{(12)}}{2} \sin k_\xi \sin k_\eta \tag{42}$$

or written in terms of the metric tensor as

$$g_{(22)} \sin^2 \frac{k_\xi}{2} + g_{(11)} \sin^2 \frac{k_\eta}{2} \geqslant \frac{g_{(12)}}{2} \sin k_\xi \sin k_\eta \tag{43}$$

Since $g_{12} = 0$, for orthogonal grids, the scheme is unconditionally stable for orthogonal grids. For the non-orthogonal grids used in this study (Table I), Equation (43) was also satisfied.

5. TWO-DIMENSIONAL WAVE DEFORMATION ANALYSIS

The amplitude and phase components of the Fourier series representing the computed wave are compared with the real solution using the complex Propagation factor [5]. The complex propagation factor gives the relation between the computed and real waves, in terms of their amplitudes and phases after a certain time interval, thus providing an estimate of the accuracy of the numerical scheme.

The change in amplitude and phase lag of wave from its original value, as time advances from t to $t + \mathrm{d}t$ is given by its eigenvalue (λ). The eigenvalue of the analytical wave is given by

$$\lambda = \mathrm{e}^{(\pm\, \mathrm{i}\omega\, \mathrm{d}t)} \tag{44}$$

Taking the analytical frequency of the two-dimensional system from Equation (17), the eigenvalue of the analytical solution is given by

$$\lambda = \mathrm{e}^{\pm\left(\frac{\mathrm{i}\, \mathrm{d}t\, c\sqrt{s_3}}{R}\right)} \tag{45}$$

The propagation factor, $T(k_\xi, k_\eta)$ is defined as the complex ratio of the computed wave in amplitude and phase to the physical wave after a time interval in which the physical wave propagates over one wavelength. The modulus of the propagation factor is a measure of the dissipation of the computed wave. The argument of the propagation factor gives a measure of the dispersion or phase lag of the computed wave, relative to the real wave. The propagation factor thus can be expressed as

$$T(k_\xi, k_\eta) = \frac{\mathrm{e}^{\mathrm{i}(\omega' t + k_{\mathrm{eq}})}}{\mathrm{e}^{\mathrm{i}(\omega t + k_{\mathrm{eq}})}} \tag{46}$$

where $k_{\mathrm{eq}} = \sqrt{k_\xi^2 + k_\eta^2}$, $t = 2\pi/\omega$ and ω and ω' are the frequencies of the analytical and the numerical waves, respectively.

Equation (46) can also be written as

$$T(k_\xi, k_\eta) = \mathrm{e}^{2\pi\, \mathrm{i}(\omega'/\omega - 1)} \tag{47}$$

The phase lag of the propagation factor can be expressed as

$$\arg(T(k_\xi, k_\eta)) = 2\pi \left\{ \frac{\tan^{-1}[\mathrm{Im}(\lambda)/Re(\lambda)]}{c\sqrt{s_3}/R} - 1 \right\} \tag{48}$$

The propagation of a physical wave having a frequency of ω over its wavelength L requires, $v = 2\pi/\omega\, \mathrm{d}t = 2\pi/\omega$ time steps, where ω is the frequency of the analytical solution given by Equation (17).

The modulus of the propagation factor is given by

$$|T(k_\xi, k_\eta)| = \left(\frac{|\lambda_{\mathrm{num}}|}{|\lambda_{\mathrm{ana}}|}\right)^v = |\lambda_{\mathrm{num}}|^v \tag{49}$$

since the modulus of the eigenvalue of the analytical solution is unity.

6. NUMERICAL EVALUATION OF PHASE SPEED AND GROUP SPEED FOR DIFFERENT GRID CONFIGURATIONS

The phase and group speed properties of different BFC grids, each having a uniform grid non-orthogonality angle (γ), are numerically evaluated using the expressions developed in Section 3.3. Four grids, with grid angles (γ) of 90, 60, 50 and 30° were used for the analysis. It is assumed that the grids are uniformly skewed and extend to infinity. Table I gives the values of the various grid quality parameters namely, the interior grid angle (γ), the elements of metric tensor ($g_{(i,j)}$), the Jacobian (J) and the aspect ratio (A) for the four grids. The angle of grid non-orthogonality (γ) or interior angle of the grid (Figure 1), as it is called from now on, can be defined as

$$\cos\gamma = \frac{g_{(12)}}{\sqrt{g_{(11)}g_{(22)}}} \tag{50}$$

The aspect ratio (A), gives the degree of distortion of the grid and is defined as

$$A = \sqrt{\frac{g_{(22)}}{g_{(11)}}} \tag{51}$$

The expressions for phase and group speeds in the transformed plane for the continuous and discrete cases given in Section 3.3 are used to evaluate the phase speed and group speed properties of a boundary fitted grid, as a function of the grid non-orthogonality angle. It can be seen from the expressions for phase and group speeds, in the continuous system, that they are dependent on the grid configuration, being used. In other words, the phase and group speeds in the continuous system are different for grids with different interior grid angles. The phase and group speeds are computed for wave numbers ranging from 0 to $\pi/2$, which corresponds to a number of grids per wavelength ranging from infinity to 4 for orthogonal grids.

The depth of water D is taken to be 10 m for calculating the wave celerity c. It is to be noted that the phase and group speeds calculated in this study, do not have any physical significance, since these values are evaluated in the transformed plane. The normalized phase

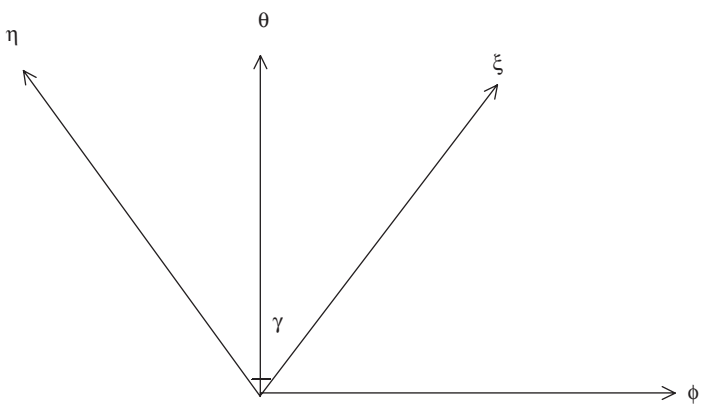

Figure 1. Definition sketch.

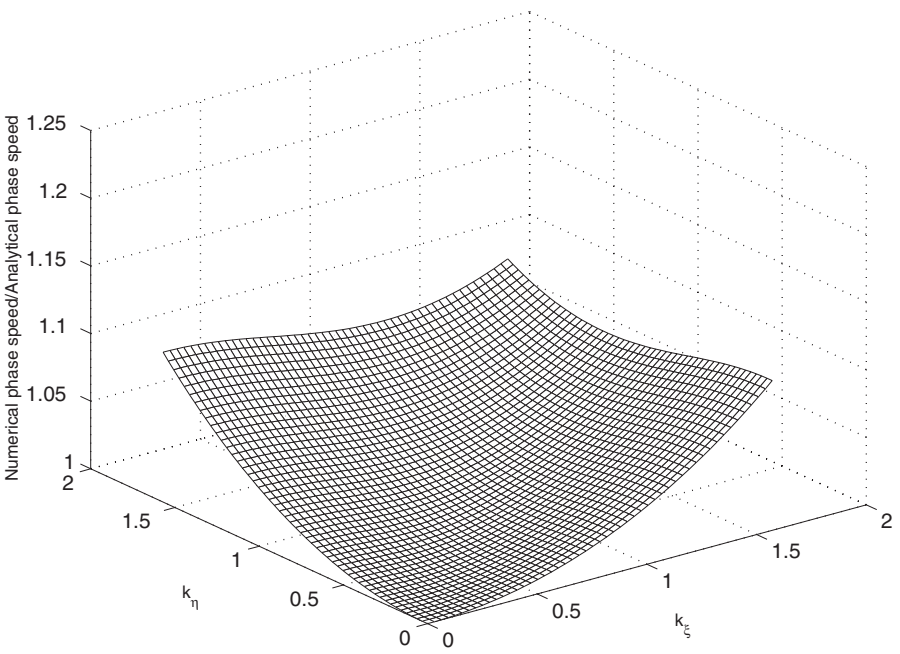

Figure 2. Contours of normalized phase speeds with $\gamma = 90°$.

speed, defined as the ratio of the phase speed of the numerical wave to that of the analytical wave is computed and it is used as one measure to estimate the accuracy of the solution. The contours of normalized phase speed, as a function of the wave number in the ξ direction (k_ξ) and wave number in the η direction (k_η) for grids with grid angles of 90, 60, 50 and 30°, are, respectively, shown in Figures 2–5. Figures 2–5 clearly show that the error in phase speed increases as the grid angle decreases from 90 to 30°. The contours of normalized group speed as function of wave numbers in the ζ and η directions (k_ξ and k_η) for grids with grid angles of 90, 60, 50 and 30°, are respectively shown in Figures 6–9. As in the case of phase speeds, the error in group speed increases as the grid angle decreases from 90 to 30°.

It is clearly seen that the error in the phase and group speeds between the analytical solution and the spatially discrete system is less than 3% for wave numbers up to 0.4. However, the error in the phase and group speeds between the analytical and numerical solutions at higher wave numbers is found to increase as the interior angle of the grid decreases.

7. ANALYSIS OF NUMERICAL STABILITY AND EVALUATION OF EIGENVALUES FOR DIFFERENT GRID CONFIGURATIONS

It is seen from a stability analysis of a three-time level scheme that it has six eigenmodes, all of which are physical, out of which one is neutral with $\lambda = 1$, another one has a dampening with a value of $\lambda = 1/3$. A numerical evaluation of rest of the modes clearly shows that they are physical and dampening modes, with magnitudes less than 1.

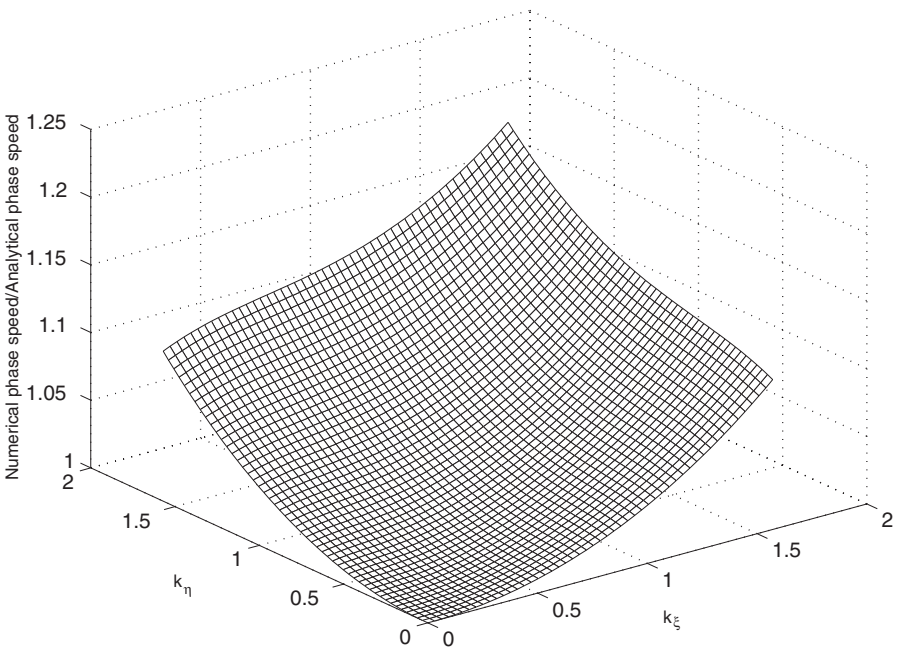

Figure 3. Contours of normalized phase speeds with $\gamma = 60°$.

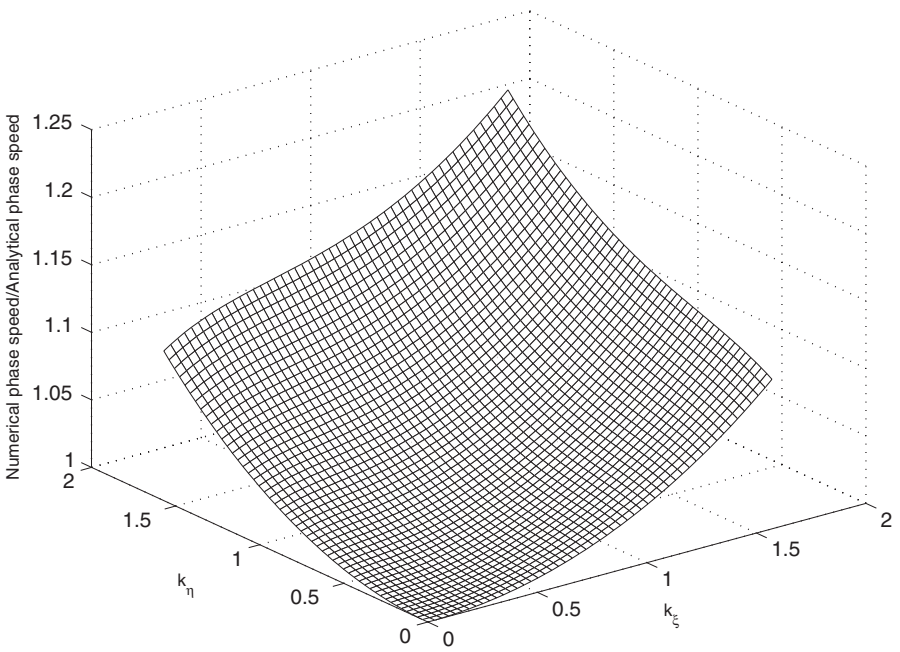

Figure 4. Contours of normalized phase speeds with $\gamma = 50°$.

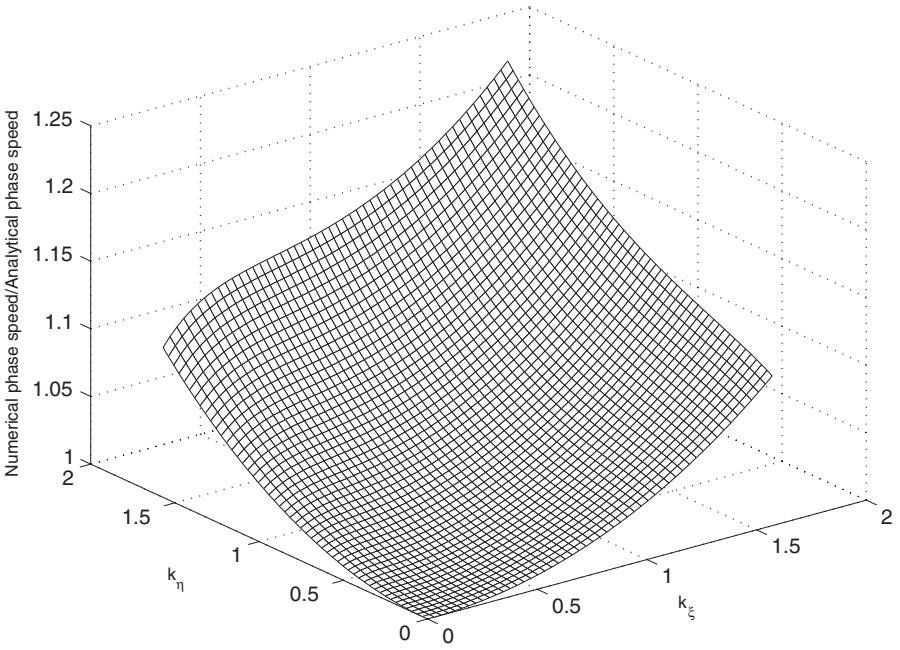

Figure 5. Contours of normalized phase speeds with $\gamma = 30^\circ$.

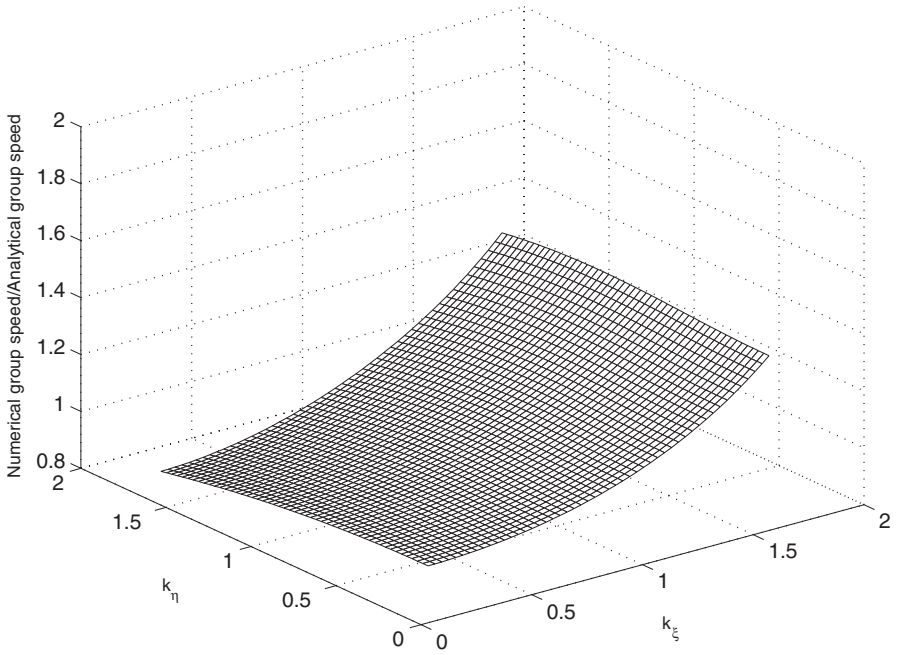

Figure 6. Contours of normalized group speeds with $\gamma = 90^\circ$.

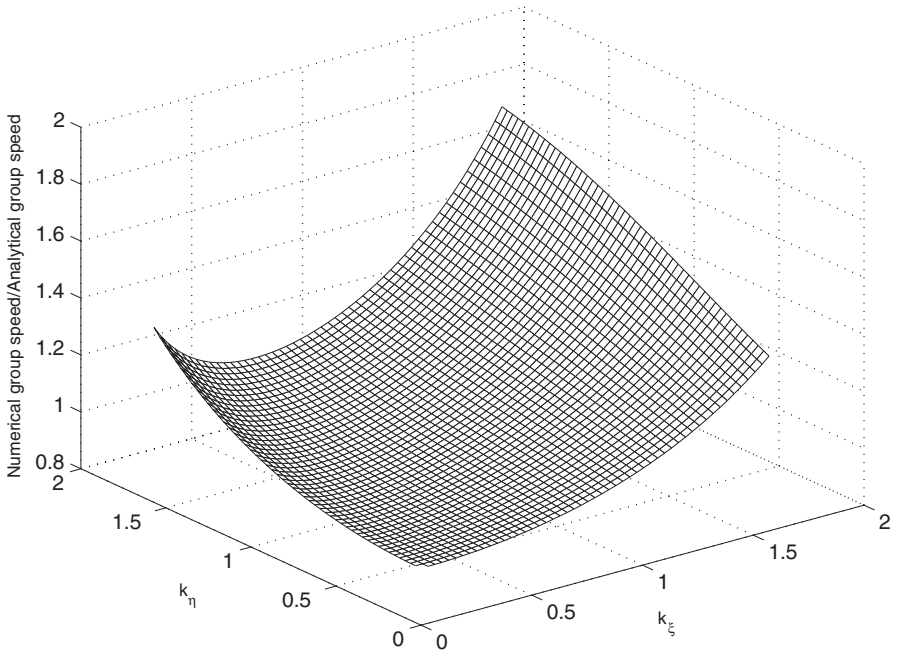

Figure 7. Contours of normalized group speeds with $\gamma = 60^\circ$.

The modulus of eigenvalues is found to be less than 1 for all the eigenmodes, for the range of wave numbers and Courant numbers studied, even for grids with a grid angle as low as 30° implying the unconditional stability characteristics of this scheme. The Courant number is defined as $(c\Delta t)/(\Delta x)$, where c is the wave celerity, D is the total water depth, Δx is the grid spacing and Δt is the time step.

The analytical stability criteria for the Crank–Nicolson derived for a non-orthogonal boundary fitted co-ordinate system is found to be satisfied for all the grids used in this study. All the three eigenmodes for this scheme are neutral, once the stability criteria is satisfied. A numerical calculation of the all eigenvalues confirmed that the modulus of eigenvalues for the Crank–Nicolson scheme is unity, irrespective of the grid angle and the Courant number. In the case of neutral modes, the amplitude of the solution remains constant, just as that of the true solution.

8. WAVE DEFORMATION ANALYSIS FOR DIFFERENT GRID CONFIGURATIONS

An evaluation of the numerical dispersion of the fully discretized equations was performed using the complex propagation factor developed by Leendertse [5]. The eigenvalues of the two numerical schemes calculated using the expressions developed in Section 3.4 are used to compute the complex propagation factor $T(k_\xi k_\eta)$, using the expressions developed in Section 3.5. The complex propagation factor $T(k_\xi k_\eta)$, is defined as the complex ratio of the eigenvalue of the numerical scheme to that of the analytical wave, as the analytical wave propagates

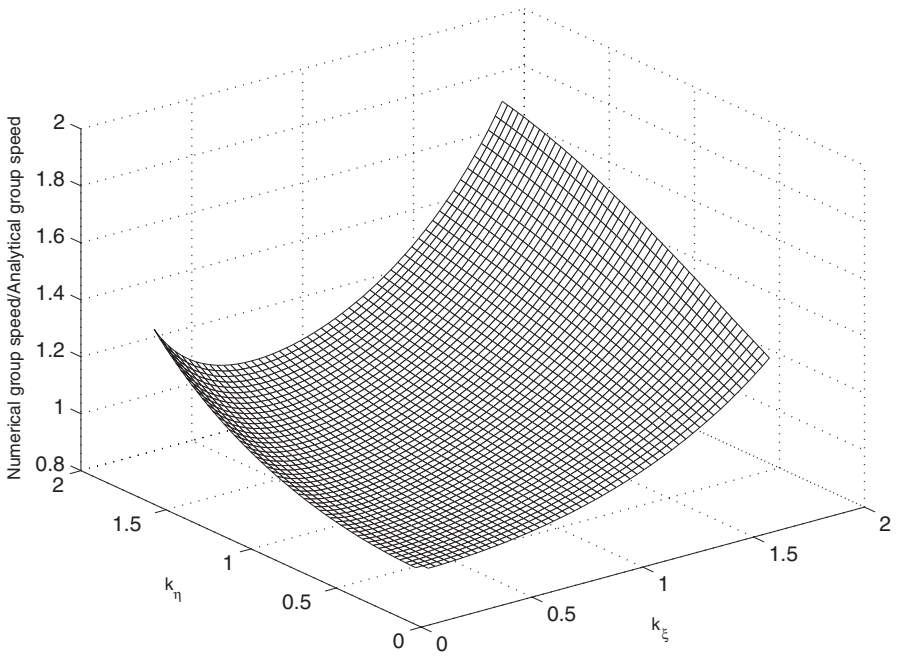

Figure 8. Contours of normalized group speeds with $\gamma = 50°$.

over one wavelength. The modulus of the complex propagation factor gives a measure of the numerical dissipation or amplitude error of the numerical scheme with respect to the analytical solution and its phase gives a measure of the numerical dispersion or phase error of the numerical scheme with respect to the analytical solution.

The modulus of propagation factor for Crank–Nicolson scheme is unity, irrespective of the grid angle and the Courant number, thus there is no dissipation of the amplitude of the solution. The contours of phase lags of the propagation factor as a function of wave numbers in the ξ and η directions (k_ξ and k_η) for a time step of 283.3 s, corresponding to a Courant number of 5 for grids with grid angles of 90, 60, 50 and 30°, respectively, are shown in Figures 10–13. It is seen that phase lag of the propagation factor increases, as the grid angle decreases from 90 to 30°. The contours of phase lags of the propagation factor as a function of wave numbers in the ξ and η directions (k_ξ and k_η) for a time step of 28.8 s, corresponding to a Courant number of 0.5 for grids with grid angles of 90, 60, 50 and 30°, respectively, are shown in Figures 14–17. It is seen that phase lag of the propagation factor increases, as the grid angle decreases from 90 to 30°.

It can be seen that the phase lag of the propagation factor increases as the Courant number increases from 1 to 5 and as the grid angle decreases from 90 to 30°. The error is significant for Courant numbers greater than 1 and grid angles less than 50°. The Crank–Nicolson scheme does not dissipate the amplitude of the solution, due to its unit modulus of the propagation factor. The error in phase lag or numerical dispersion for the Crank–Nicolson scheme is very low for Courant numbers less than 1, thus making it an ideal candidate for the numerical solution of shallow water equations. Crank–Nicolson scheme has an added advantage that its two eigenvalues have identical dissipative and dispersive characteristics.

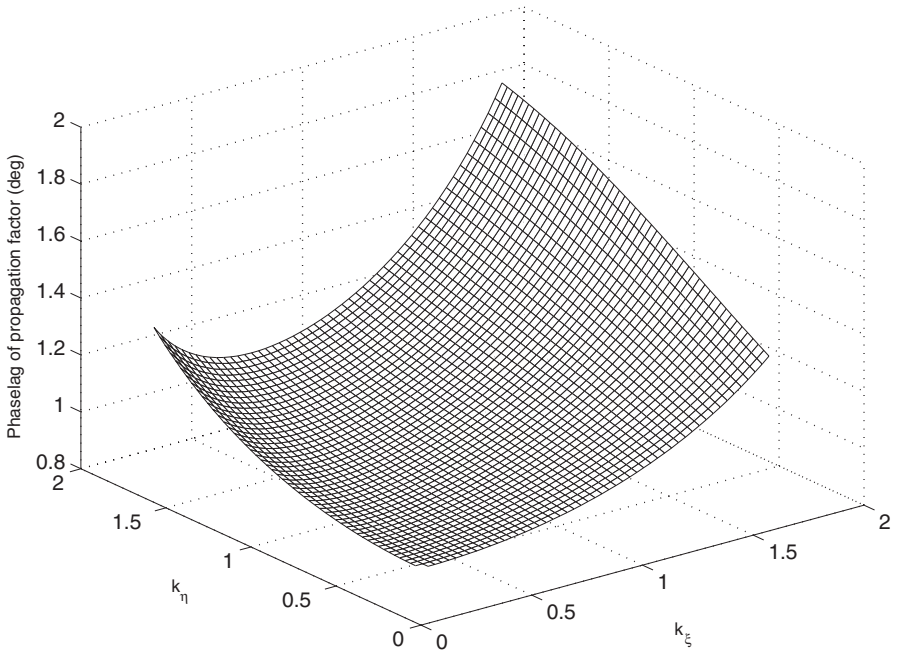

Figure 9. Contours of normalized group speeds with $\gamma = 30^\circ$.

Even though the Crank–Nicolson scheme is less dissipative and dispersive compared to the three-time level scheme, comparison of the solutions obtained for the case of tidal forcing in a rectangular channel, open at one end [1] indicate that both the schemes have the same accuracy, for orthogonal and slightly non-orthogonal grids. However, oscillations are found to develop with the Crank–Nicolson scheme for grids with grid angles below 50°. These oscillations remain, since there is no mechanism to dissipate them.

9. CONCLUSIONS

The dispersion and stability analyses for the linearized shallow water equations, in a non-orthogonal boundary-fitted co-ordinate system, discretized using a second-order finite differences on an Arakawa-C grid, are carried out in the transformed domain. The phase speed and group speeds for the discrete system, with different grid configurations are compared with those obtained for the continuous system.

The error in phase and group speeds between the analytical solution and the spatially discrete system is negligible, even for grids with a grid angle as low as 30°, for wave numbers ranging from 0 to $\pi/2$, which correspond to a grids per wavelength ranging from infinity to 4. However, the error in phase and group speeds between the analytical solution and the spatially discrete system for higher wave numbers is found to increase, as the grid angle decreases from 90 to 30°. Thus, the spatially discrete system is seen to be slightly dispersive with the degree of dispersivity increasing with an decrease in grid angle or grid resolution and these

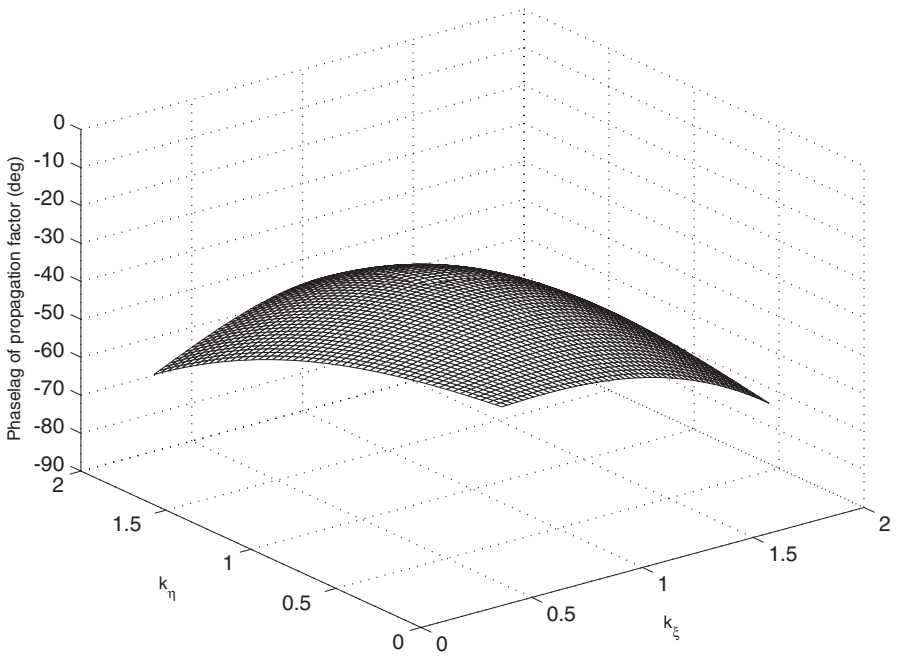

Figure 10. Contours of phase lag of propagation factor for λ_1 in Crank–Nicolson scheme with $\mathrm{d}t = 283.3$ s for $\gamma = 90°$.

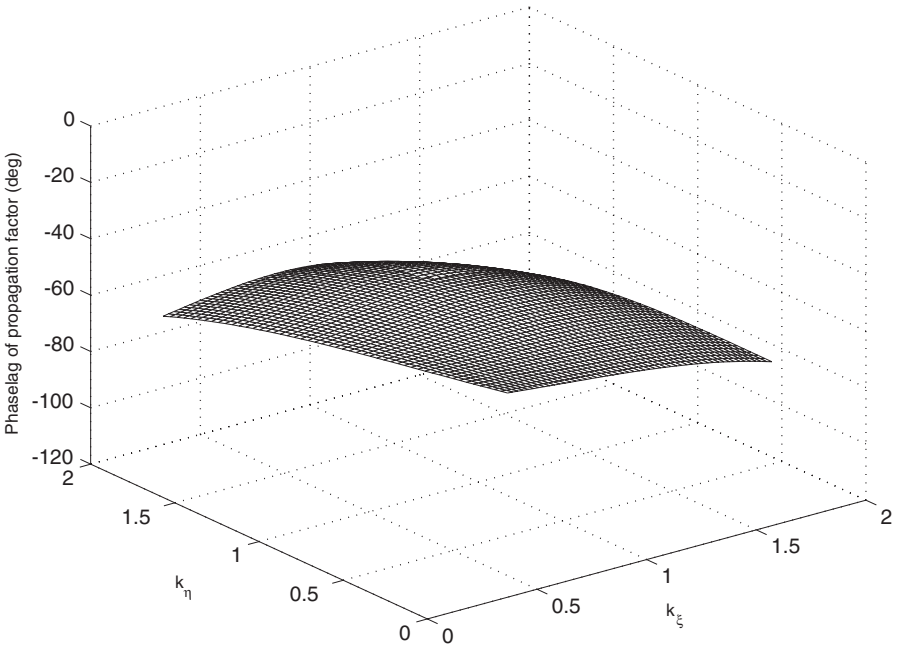

Figure 11. Contours of phase lag of propagation factor for λ_1 in Crank–Nicolson scheme with $\mathrm{d}t = 283.3$ s for $\gamma = 60°$.

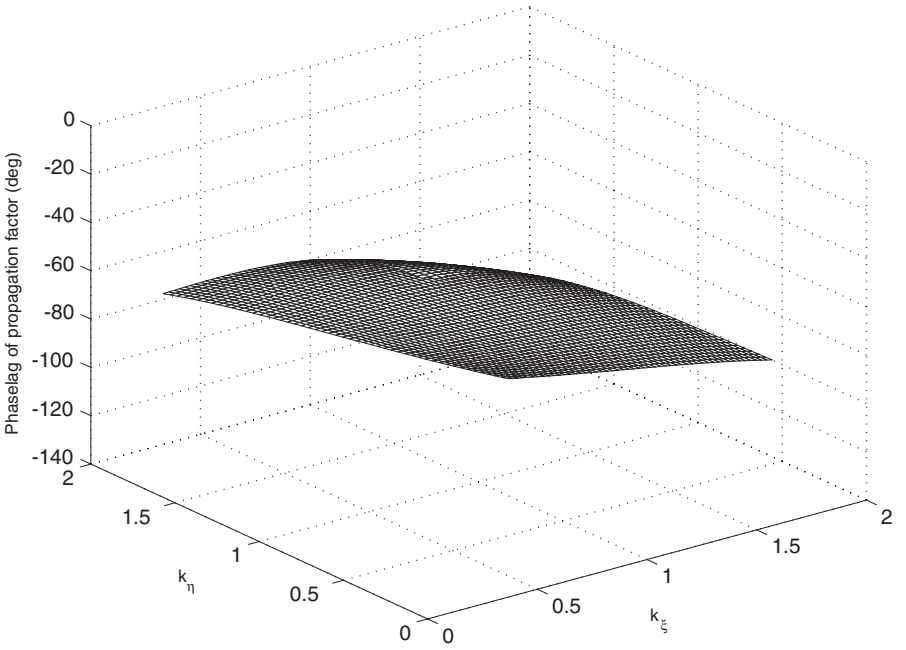

Figure 12. Contours of phase lag of propagation factor for λ_1 in Crank–Nicolson scheme with $\mathrm{d}t = 283.3$ s for $\gamma = 50^\circ$.

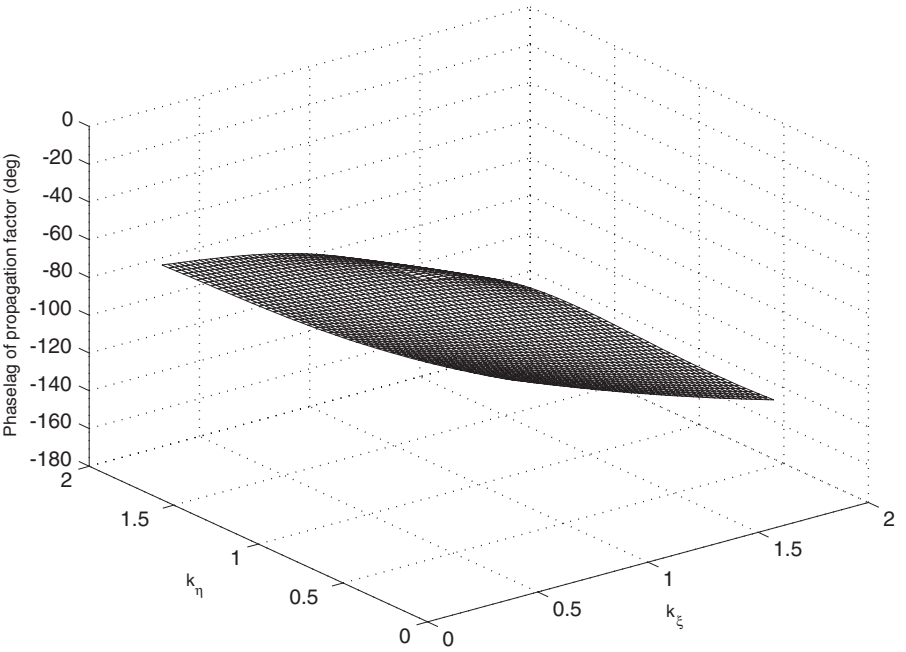

Figure 13. Contours of phase lag of propagation factor for λ_1 in Crank–Nicolson scheme with $\mathrm{d}t = 283.3$ s for $\gamma = 30^\circ$.

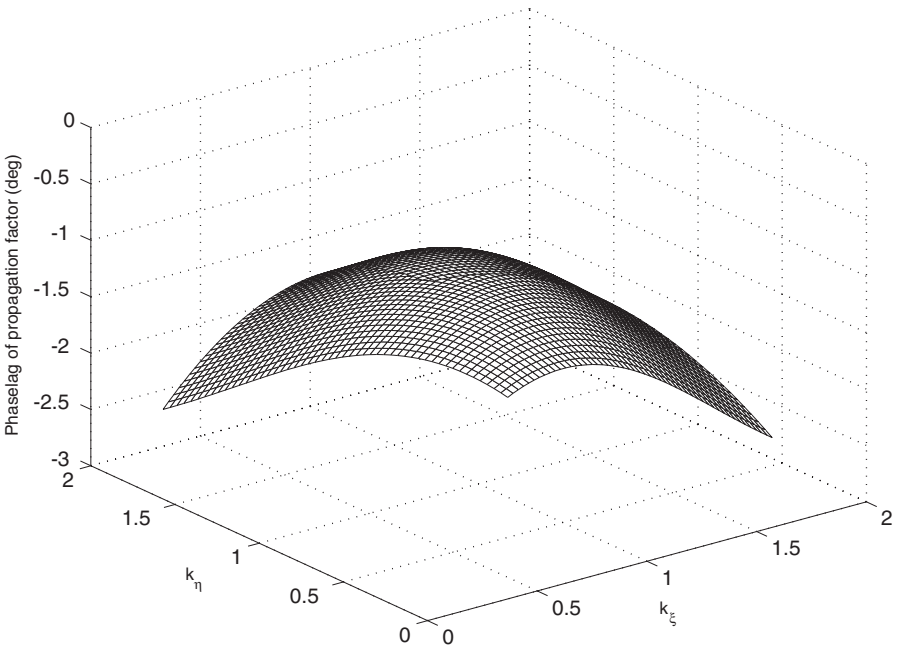

Figure 14. Contours of phase lag of propagation factor for λ_1 in Crank–Nicolson scheme with $\mathrm{d}t = 28.3$ s for $\gamma = 90°$.

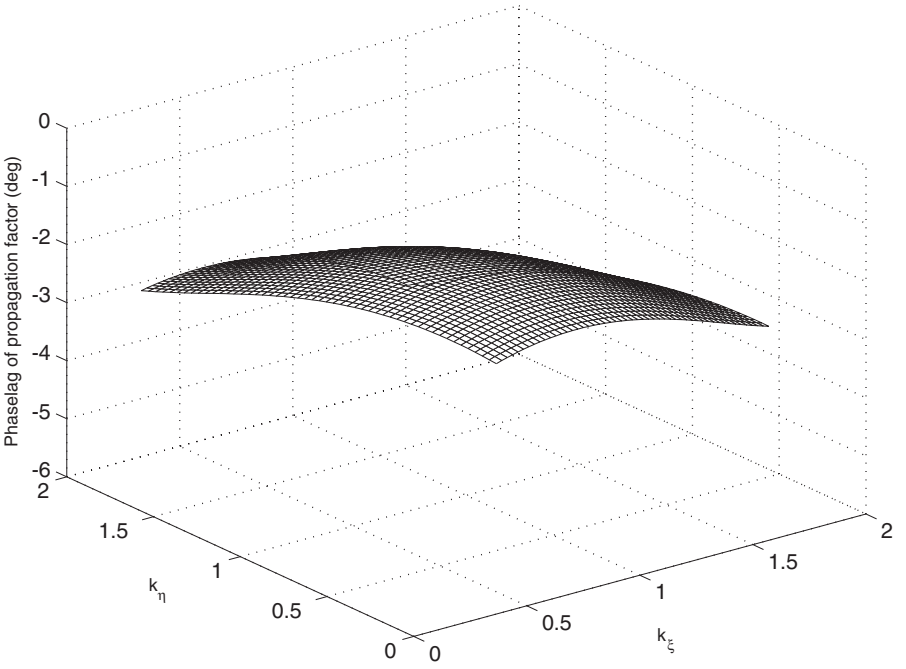

Figure 15. Contours of phase lag of propagation factor for λ_1 in Crank–Nicolson scheme with $\mathrm{d}t = 28.3$ s for $\gamma = 60°$.

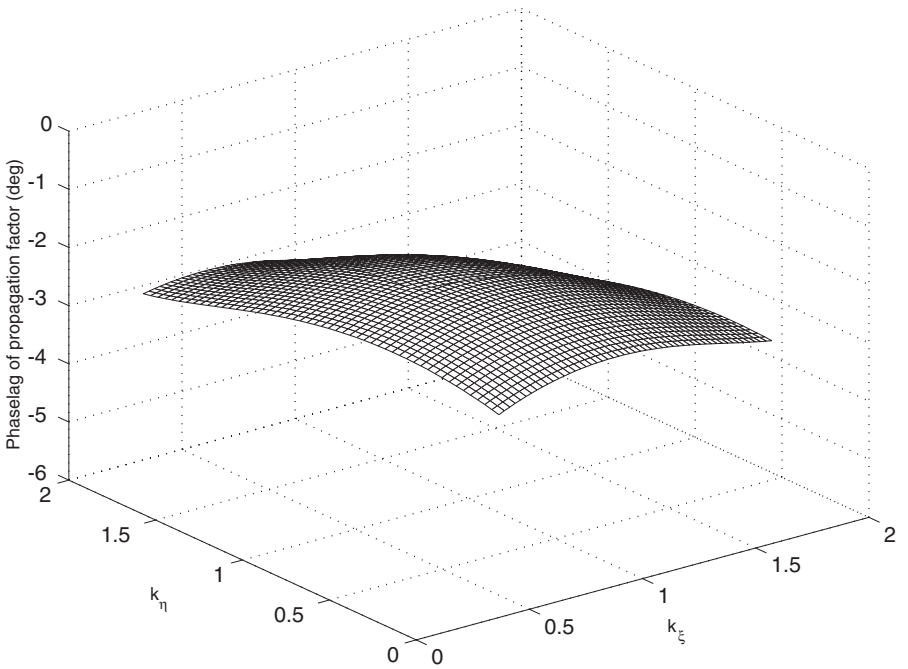

Figure 16. Contours of phase lag of propagation factor for λ_1 in Crank–Nicolson scheme with $\mathrm{d}t = 28.3$ s for $\gamma = 50°$.

results are in agreement with the conclusions reached by Sankaranarayanan and Spaulding [1]. Sankaranarayanan and Spaulding [1] found through model testing with analytical solutions that the error in the model predicted velocities increases, as the grid angle deviates from orthogonality. They also established through truncation error analysis that the error increases, as the grid angle deviates from orthogonality.

A Von-Neumann stability analysis of a three-time level scheme used by Muin and Spaulding [6] shows that the scheme is stable even for highly non-orthogonal grids and at high Courant numbers. The scheme has been found to possess six physical modes. The modulus of eigenvalues for all the modes were found to be less than 1, indicating that the scheme is unconditionally stable.

A Von-Neumann stability analysis of the two-time level Crank–Nicolson scheme shows it to be unconditionally stable for the orthogonal grids and conditionally stable for non-orthogonal grids. The stability criteria for the non-orthogonal BFC grids is found to be satisfied for grids with angle of non-orthogonality as low as 30°. The scheme has three physical modes, which are neutral, subject to the satisfaction of the stability criteria. The modulus of the eigenvalue is found to be one for all wave numbers, irrespective of the grid angle and the value of the Courant number.

The amplitude and phase errors of the fully discretized equations, using a two-time level Crank–Nicolson scheme is calculated based on the complex propagation factor. The modulus of the complex propagation factor at high Courant numbers is found to be unity even for grids with a grid angle as low as 30°. Thus, there is no dissipation of the amplitude of the solution

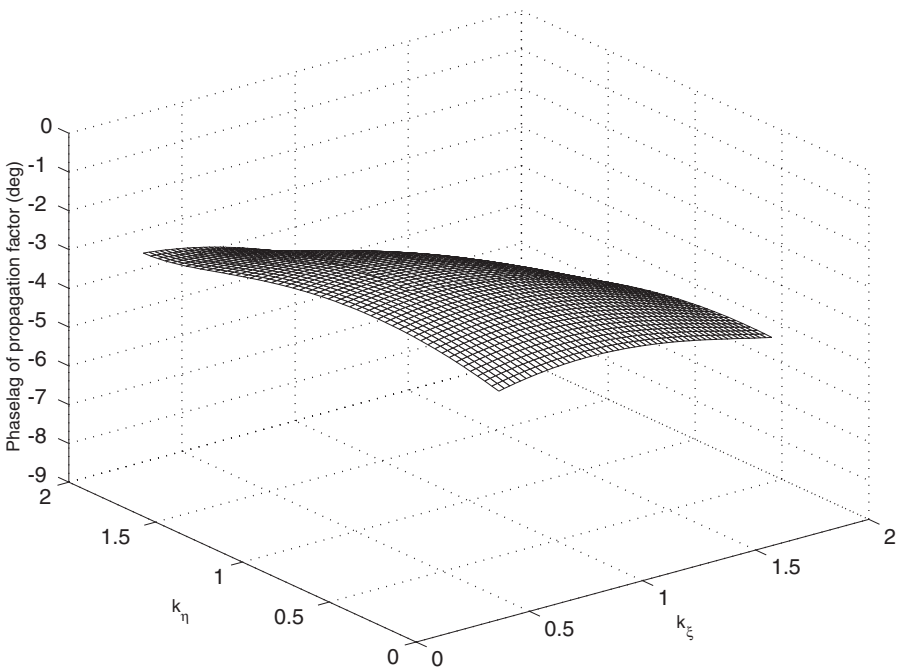

Figure 17. Contours of phase lag of propagation factor for λ_1 in Crank–Nicolson scheme with $dt = 28.3$ s for $\gamma = 30°$.

for the Crank–Nicolson scheme for grids with low grid angles and at high Courant numbers. The phase lag of the propagation factor is found to increase as the grid angle decreases from 90 to 30°. The phase lag of the propagation factor is also found to decrease as the Courant number decreases from 5 to 0.5. The phase lag of the propagation factor for this scheme is found to be less than 10° for Courant numbers less than 1, even for grids with grid angles as low as 30°. Two of the three modes in this scheme are found to possess identical dissipative and dispersive characteristics.

ACKNOWLEDGEMENTS

S. Sankaranarayanan thanks the University of Rhode Island (URI) for providing him a Graduate fellowship for a year.

REFERENCES

1. Sankaranarayanan S, Spaulding ML. A study of the effects of grid non-orthogonality on the solution of shallow water equations in boundary-fitted co-ordinate systems. *Journal of Computational Physics* 2003; **184**:299–320.
2. Arakawa A, Lamb VR. Computational design of the basic dynamical processes of the ULCA general circulation model. *Methods in Computational Physics* 1977; **17**:173–265.
3. Foreman MGG. A two-dimensional dispersion analysis of selected methods for solving linearized shallow water equations. *Journal of Computational Physics* 1984; **56**:287–223.
4. Song Y, Tang T. Dispersion and group velocity in numerical schemes for three-dimensional hydrodynamic equations. *Journal of Computational Physics* 1993; **105**:72–82.

5. Leendertse JJ. Aspects of computational model for long period water wave propagation. *Report RM*-5294-PR, The Rand Corp., Santa Monica, CA, 1967.
6. Muin M, Spaulding ML. Two-dimensional boundary-fitted circulation model in spherical co-ordinates. *Journal of Hydraulic Engineering ASCE* 1996; **122**(9):512–521.
7. White FM. *Viscous Fluid Flow*. McGraw Hill: New York, 1991.
8. Sankaranarayanan S, Spaulding ML. Dispersion and stability analyses of the linearized two-dimensional shallow water equations in cartesian co-ordinates. Department of Ocean Engineering, University of Rhode Island, Narragansett, 2001.

